Dynamic phase transition in the kinetic spin-1 Blume-Capel model under a time-dependent oscillating external field

Mustafa Keskin and Osman Canko
Department of Physics, Erciyes University, 38039 Kayseri, Turkey

Ümit Temizer
Department of Physics, Erciyes University, 66100 Yozgat, Turkey

(Received 23 February 2005; revised manuscript received 21 April 2005; published 27 September 2005)

We study within a mean-field approach the stationary states of the kinetic spin-1 Blume-Capel model in the presence of a time-dependent oscillating external magnetic field. We use the Galuber-type stochastic dynamics to describe the time evolution of the system. We have found that the behavior of the system strongly depends on the crystal field interaction D. We have obtained two types of solutions: a symmetric one, which corresponds paramagnetic phase where the magnetization (m) of the system oscillates in time around zero, and an antisymmetric one where m oscillates in time around a finite value different from zero. There are regions of the phase space where both solutions coexist. The dynamic phase transition from one regime to the other can be a first- or a second-order depending on the region in the phase diagram. Hence, the system exhibits one or more dynamic tricritical point, which depends on the values D. We also calculate the Liapunov exponent to verify the stability of the solutions and the dynamic phase transition points.

DOI: 10.1103/PhysRevE.72.036125 PACS number(s): 05.50.+q, 05.70.Fh, 64.60.Ht, 75.10.Hk

I. INTRODUCTION

The spin-1 Ising model with a crystal field interaction or single-ion anisotropy is often called the Blume-Capel (BC) model, was first introduced by Blume [1] and independently by Capel [2]. The model has been subject of many theoretical studies since its introduction [1,2] nearly 40 years ago, because it plays a fundamental role in the multicritical phenomena associated with various physical systems, such as multicomponent fluids, ternary alloys, and magnetic systems. The mean-field (MF) approximation [1–3] was the original technique used to obtain an approximate solution to the model, but since then it has been studied by a variety of techniques in the equilibrium statistical physics such as the high- and low- temperature series expansions [4], a Green's functions diagrammatic approach [5], Monte Carlo simulations [6], renormalization group calculations [7], the effective field theory [8], the cluster-variation method [9], nonperturbative approach based on a thermodynamical self-consistent [10], and the expanded Bethe-Peierls approximation [11]. Recently, model has been also solved by using the exact recursion equations on the Bethe lattice [12].

Thus, although a great amount is known about the equilibrium properties of the spin-1 BC model, the nonequlibrium properties of the model have not been as thoroughly explored. Fiig *et al.* [13] used dynamical Monte Carlo simulations to study dynamical behavior of the metastable states in the BC model and found that the decay of a particular metastable state might happen either directly or via a succession of separate steps, depending on the availability and relative stability of a second metastable state intermediate between the initial one and the equilibrium phase. Manzo and Olivieri [14] have used this model to study the metastability and nucleation by also using dynamical Monte Carlo simulations. Ekiz *et al.* [15] have studied dynamics of the BC model by using the path probability method with point distribution [16], in order to investigate how to obtain the metastable phases with the long-range-order parameters and as well as to see the "flatness" property of the metastable state and the unstable state. They have also calculated the phase transitions of the metastable and the unstable branches of the order parameters besides the stable branches and have presented the complete phase diagram.

In this paper, we study within a mean-field approach the stationary states of the kinetic spin-1 BC model described by the Glauber dynamic [17] in the presence of a time-dependent oscillating external magnetic field. Especially, we investigate the time dependence of magnetization and the behavior of the average magnetization as a function of the reduced temperature and the reduced external magnetic field (h). In these studies, we obtain the dynamic phase transition (DPT) points and present the phase diagrams of the system in the (T,h) plane. We also calculate the Liapunov exponent to verify the stability of solutions and the DPT points. This type of calculation was first applied to a kinetic spin-1/2 Ising system by Tomé and Oliveira [18] and was then used to study kinetics of a classical mixed spin-1/2 and spin-1 Ising system by Buendía and Machado [19]. They also presented only two phase diagrams in the (T,h) plane for the BC model, but they did not study the BC model in detail. One of these two phase diagrams was incomplete; i.e., they missed a very important part of the phase diagram due to the reason that they did not make the calculations for higher values of h. Moreover, Buendía and Machado [19] did not verify the stability of solutions by calculating the Liapunov exponent. We should also mention that one of the defects of this type of calculation or method is the absence of the fluctuations. In spite of this defect, the method is an adequate starting point. Within this method, it is easy to investigate the behavior of the time variation of the magnetization and the behavior of

the average magnetization as a function of reduced temperature. Moreover, one can calculate the DPT points easily and present the phase diagrams by using this method.

It is worthwhile to mention that the DPT was first found in the study of the deterministic mean-field equation of motion for the ferromagnetic system in an oscillating field [18,20], and it was followed by Monte Carlo simulation researches of kinetic spin-1/2 Ising models [21–23], as well as by further mean-field studies [19,24]. Moreover, recently, Tutu and Fujiwara [25] developed a systematic method for obtaining the phase diagrams in DPTs, and constructed a general theory of DPTs near the transition point based on a mean-field description, such as Landau's general treatment of the equilibrium phase transitions. DPT may also have been observed experimentally in ultrathin Co films on Cu(100) [26]. Reviews of earlier research on the DPT and related phenomena are found in Ref. 23.

The remainder of this paper is organized as follows. In Sec. II, the BC model is presented briefly. In Sec. III, the derivation of the mean-field dynamic equations of motion is given by using a Glauber-type stochastic dynamics in the presence of a time-dependent oscillating external magnetic field. In Sec. IV, the DPT points are calculated and the phase diagrams presented. Section V contains the summary and conclusions.

II. THE MODEL

The BC model consisting of a spin-1 Ising Hamiltonian with a crystal field interaction or a single-ion anisotropy is one of the most extensively studied models in statistical physics and condensed matter physics, and the model is defined by the Hamiltonian

$$\mathcal{H} = -J\sum_{\langle ij\rangle} S_i S_j - D\sum_i S_i^2 - H\sum_i S_i, \tag{1}$$

where the S_i takes the value ± 1 or 0 at each site i of a lattice and $\langle ij\rangle$ indicates summation over all pairs of nearest neighbor sites. J is the bilinear exchange interaction parameter, D is the crystal field interaction or a single-ion anisotropy, and H is a time-dependent external oscillating magnetic field. H is given by

$$H(t) = H_0 \cos(wt), \tag{2}$$

where H_0 and $w=2\pi\upsilon$ are the amplitude and the angular frequency of the oscillating field, respectively. The system is in contact with an isothermal heat bath at absolute temperature.

III. DERIVATION OF MEAN-FIELD DYNAMIC EQUATIONS

The system evolves according to a Glauber-type stochastic process at a rate of $1/\tau$ transitions per unit time. We define $P(S_1,S_2,\ldots,S_N;t)$ as the probability that the system has the S-spin configuration, $S_1,S_2,\ldots,S_N$, at time t. The time dependence of this probability function is assumed to be governed by the master equation that describes the interaction between spins and heat bath, and can be written as

$$\begin{aligned}\frac{d}{dt}P(S_1,S_2,\ldots,S_N;t) = &-\sum_i \left[\sum_{S_i\neq S_i'} W_i(S_i\to S_i')\right] \\ &\times P(S_1,S_2,\ldots,S_i,\ldots,S_N;t) \\ &+\sum_i \left[\sum_{S_i\neq S_i'} W_i(S_i'\to S_i) \right. \\ &\left. \times P(S_1,S_2,\ldots,S_i',\ldots,S_N;t)\right],\end{aligned} \tag{3}$$

where $W_i(S_i\to S_i')$, the probability per unit time that the ith spin changes from the value S_i to S_i', and in this sense the Glauber model is stochastic. Since the system is in contact with a heat bath at absolute temperature T, each spin can change from the value S_i to S_i' with the probability per unit time

$$W_i(S_i\to S_i') = \frac{1}{\tau}\frac{\exp[-\beta\Delta E(S_i\to S_i')]}{\sum_{S_i'}\exp[-\beta\Delta E(S_i\to S_i')]}, \tag{4}$$

where $\beta=1/k_BT$, and k_B is the Boltzmann factor, $\Sigma_{S_i'}$ is the sum over the three possible values of S_i', ± 1, 0, and

$$\Delta E(S_i\to S_i') = -(S_i'-S_i)\left(J\sum_{\langle j\rangle} S_j + H\right) - (S_i'^2 - S_i^2)D, \tag{5}$$

gives the change in the energy of the system when the S_i-spin changes. The probabilities satisfy the detailed balance condition

$$\frac{W_i(S_i\to S_i')}{W_i(S_i'\to S_i)} = \frac{P(S_1,S_2,\ldots,S_i',\ldots,S_N)}{P(S_1,S_2,\ldots,S_i,\ldots,S_N)}, \tag{6}$$

and substituting the possible values of S_i, we get

$$W_i(1\to 0) = W_i(-1\to 0) = \frac{1}{\tau}\frac{\exp(-\beta D)}{2\cosh(\beta a)+\exp(-\beta D)}, \tag{7a}$$

$$W_i(1\to -1) = W_i(0\to -1) = \frac{1}{\tau}\frac{\exp(-\beta a)}{2\cosh(\beta a)+\exp(-\beta D)}, \tag{7b}$$

$$W_i(0\to 1) = W_i(-1\to 1) = \frac{1}{\tau}\frac{\exp(\beta a)}{2\cosh(\beta a)+\exp(-\beta D)}, \tag{7c}$$

where $a=J\Sigma_{\langle j\rangle}S_j+H$. Notice that, since $W_i(S_i\to S_i')$ does not depend on the value S_i, we can write $W_i(S_i\to S_i')=W_i(S_i')$, and the master equation becomes

$$\frac{d}{dt}P(S_1,S_2,\ldots,S_N;t) = -\sum_i \left(\sum_{S_i'\neq S_i} W_i(S_i')\right)P(S_1,S_2,\ldots,S_i,\ldots,S_N;t) + \sum_i W_i(S_i)\left(\sum_{S_i'\neq S_i} P(S_1,S_2,\ldots,S_i',\ldots,S_N;t)\right). \quad (8)$$

Since the sum of probabilities is normalized to one, by multiplying both sides of Eq. (8) by S_k and taking the average, we obtain

$$\tau\frac{d}{dt}\langle S_k\rangle = -\langle S_k\rangle + \left\langle \frac{2\sinh\beta\left[J\sum_{\langle j\rangle}S_j + H\right]}{2\cosh\beta\left[J\sum_{\langle j\rangle}S_j + H\right] + \exp(-\beta D)}\right\rangle, \quad (9)$$

or, in a terms of a mean-field approach,

$$\tau\frac{d}{dt}\langle S\rangle = -\langle S\rangle + \frac{2\sinh\beta[Jz\langle S\rangle + H_0\cos(wt)]}{2\cosh\beta[Jz\langle S\rangle + H_0\cos(wt)] + \exp(-\beta D)}, \quad (10)$$

where z is the coordination number. The system evolves according to the differential equation given by Eq. (10), which can be written in the form

$$\Omega\frac{d}{d\xi}m = -m + \frac{\sinh[(1/T)(m + h\cos\xi)]}{\cosh[(1/T)(m + h\cos\xi)] + \frac{1}{2}\exp\left(-\frac{d}{T}\right)}, \quad (11)$$

where $m=\langle S\rangle$, $\xi=wt$, $T=(\beta zJ)^{-1}$, $d=D/zJ$, $h=H_0/zJ$, and $\Omega=\tau w$. We fixed $z=4$ and $\Omega=2\pi$. The solution and discussion of this equation are given in the next section.

IV. DYNAMIC PHASE TRANSITION POINTS AND PHASE DIAGRAMS

In this section, we shall find the DPT points and present the phase diagrams. For these purposes, first we have to study the stationary solutions of the dynamic equation, given in Eq. (11), when the parameters T, d, and h are varied. The stationary solution of Eq. (11) will be a periodic function of ξ with period 2π; that is, $m(\xi+2\pi)=m(\xi)$. Moreover, they can be one of two types according to whether they have or do not have the property

$$m(\xi+\pi) = -m(\xi). \quad (12)$$

A solution that satisfies Eq. (12) is called a symmetric solution, which corresponds to a paramagnetic (P) solution. In this solution, the magnetization $m(\xi)$ oscillates around the zero value and is delayed with respect to the external field. The second type of solution, which does not satisfy Eq. (12), is called a nonsymmetric solution, which corresponds to a ferromagnetic (F) solution. In this case, the magnetization

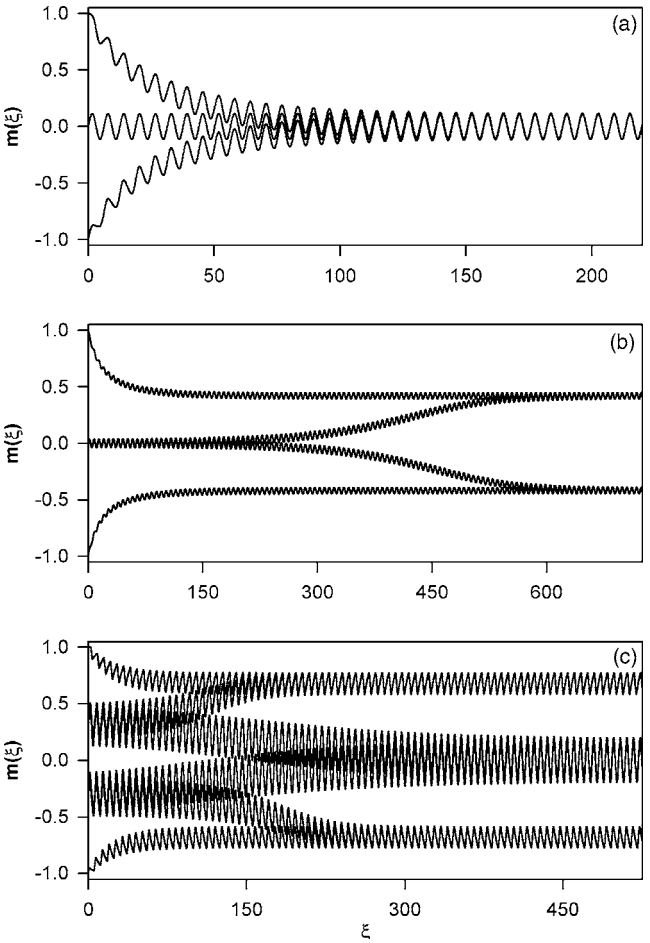

FIG. 1. Time variations of the magnetization (m): (a) Exhibiting a paramagnetic phase (P), $d=-0.25$, $h=0.5$, and $T=0.75$; (b) Exhibiting a ferromagnetic phase (F), $d=-0.25$, $h=0.2$, and $T=0.5$; (c) Exhibiting a coexistence region (F+P), $d=-0.25$, $h=0.75$, and $T=0.1$.

does not follow the external magnetic field any more, but instead of oscillating around a zero value, it oscillates around a nonzero value. These facts are seen explicitly by solving Eq. (11) numerically. Equation (11) is solved by using the numerical method of the Adams-Moulton predictor corrector method for a given set of parameters and initial values, and is presented in Fig. 1. From Fig. 1, one can see that three different solutions, namely, the paramagnetic the ferromagnetic, and the coexistence solution (P+F) in which the ferromagnetic and paramagnetic solutions coexist, exist in the system. In Fig. 1(a), only the symmetric solution is always obtained, hence we have a paramagnetic solution, but in Fig. 1(b) only the nonsymmetric solution is found; therefore, we have a ferromagnetic solution. Neither solution depends on the initial values. On the other hand, in Fig. 1(c) both the symmetric and nonsymmetric solutions always exist in the system, hence we have the coexistence solution (F+P). In this case, the solutions depend on the initial values, seen in Fig. 1(c) explicitly. We should also mention that for large values of h and the bigger values of negative d, the paramagnetic solution occurs for low values of reduced temperature. This fact will be seen the phase diagrams of the system. We

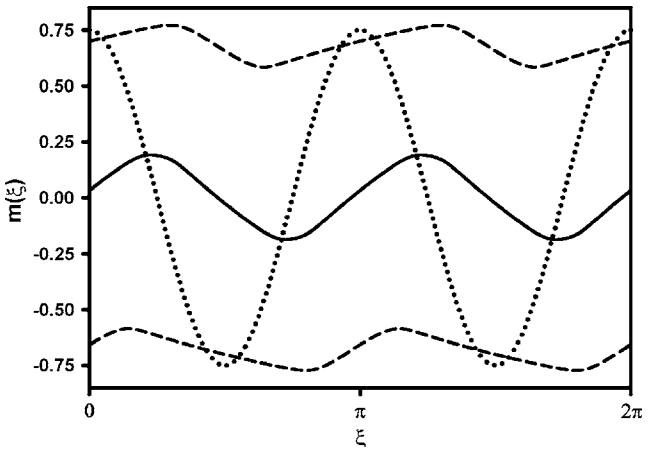

FIG. 2. Types of solutions: the dashed lines indicate the nonsymmetric solution that corresponds to a ferromagnetic phase, the solid line represents the symmetric solution that corresponds to a paramagnetic phase, and the dotted line is the input field $h\cos\xi$, $d=-0.25$, $h=0.75$, and $T=0.10$.

have also presented one more figure along the input field $h\cos\xi$ in order to clearly see the types of solutions: symmetric and nonsymmetric solutions (see Fig. 2). In the figure, the solid line denotes the symmetric solution, the dashed line corresponds to the nonsymmetric solutions, and the dotted line is the input field $h\cos\xi$.

Thus, Figs. 1 and 2 show us that we have two types of solutions: symmetric and nonsymmetric solutions. Moreover, Fig. 1 displays that a paramagnetic solution or phase, a ferromagnetic phase and the coexistence phase (F+P) exist in the system. In order to see the boundaries among these three regions, we have to calculate DPT points, and then we can present phase diagrams of the system. DPT points will be obtained by investigating the behavior of the average magnetization as a function of the reduced temperature and also the reduced external magnetic field. These investigations will be also checked and verified by calculating the Liapunov exponent.

The average magnetization (M) in a period is given as

$$M=\frac{1}{2\pi}\int_0^{2\pi} m(\xi)d\xi. \tag{13}$$

The behavior of M as a function of the reduced temperature for several values of h and d are obtained by combining the numerical methods of Adams-Moulton predictor corrector with the Romberg integration, and the results are plotted in Fig. 3 together with Liapunov exponent (λ). In the figure, the thick solid line corresponds to M and the thin line is the Liapunov exponent, which will be explained later. Figure 3(a) represents the reduced temperature dependence of the average magnetization (M) for $h=0.75$ and $d=-0.25$. In this case, M decreases to zero discontinuously as the reduced temperature increases, therefore a first-order phase transition occurs. The first-order phase transition temperature T_t, is marked with a dashed arrow in the figure: $T_t=0.1620$. Figures 3(b) and 3(c) illustrate the thermal variations of M for $h=0.725$ and $d=-0.25$ for two different initial values; i.e., the initial value of M is taken as 1 for Fig. 3(b) and zero for Fig. 3(c). In Fig. 3(b), M decreases to zero continuously as the reduced temperature increases, therefore, the system exhibits a second-order phase transition. The second-order phase transition temperature T_c is marked with a solid arrow in the figure: $T_c=0.235$. In Fig. 3(c), the system undergoes two successive phase transitions. The first one is a first-order from the paramagnetic phase to the ferromagnetic phase, and the second one is a second-order, from the (F) phase to the (P) phase: $T_t=0.1175$ and $T_c=0.2350$. This means that the coexistence region, i.e., the F+P phase, exists for $d=-0.25$ and $h=0.725$ in the system, and this fact is seen in the phase diagram of Fig. 7(b) explicitly [compare Figs. 3(b) and 3(c) with Fig. 7(b)]. Finally, Fig. 3(d) shows the behavior of M as a function of the reduced temperature for $h=0.4$ and $d=-0.25$. It is easily seen that the system undergoes only a second-order phase transition, i.e., from the F phase to the P phase at $T_c=0.4950$. At this point we should also mention that in these numerical calculations, we have taken initial values as $M=1$ or 0. Because these initial values lead to a speed-up of the whole relaxation process, especially near the phase transition temperatures. If one takes the initial values between these two values, e.g., $M=0.2$ or $M=0.4$, the system takes too long a time to relax into either the ferromagnetic or paramagnetic solutions.

Now we can check and verify the stability of solutions, and as well as the DPT points by calculating the Liapunov exponent λ. If we write Eq. (11) as

$$\Omega\frac{dm}{d\xi}=F(m,\xi), \tag{14}$$

then the Liapunov exponent λ is given by

$$\Omega\lambda=\frac{1}{2\pi}\int_0^{2\pi}\frac{\partial F}{\partial m}d\xi. \tag{15}$$

The solution is stable when $\lambda<0$. The behavior of the Liapunov exponent as a function of reduced temperature is also shown in Fig. 3, in which thin lines corresponds to the Liapunov exponents. λ_s and λ_n are the Liapunov exponents associated to the symmetric and nonsymmetric solutions, respectively. If λ_s and λ_n increases to zero continuously as the reduced temperature approaches to the phase transition temperature, the temperature where $\lambda_n=\lambda_s=0$ is the second-order phase transition temperature T_c. On the other hand, if one of λ increases to zero discontinuously and the other λ increases to zero continuously as the reduced temperature approaches the phase transition temperature, the temperature at which the discontinuity occurs first for one of the λ and the other $\lambda=0$, is the first-order phase transition temperature T_t. For example, in Fig. 3(a) $\lambda_n=0$ and the discontinuity occurs for λ_s, in which the temperature where this discontinuity occurs is T_t, but in Fig. 3(c) $\lambda_s=0$ and discontinuity occurs for λ_n. Moreover, if one compares the behavior of M and λ in Fig. 3, one can see that T_t and T_c found by using the both calculations are exactly the same.

We also investigate the behavior of the average magnetization as a function of the reduced external magnetic field (h) for $d=-0.25$; $T=0.162$, $T=0.235$, $T=0.1175$, and T

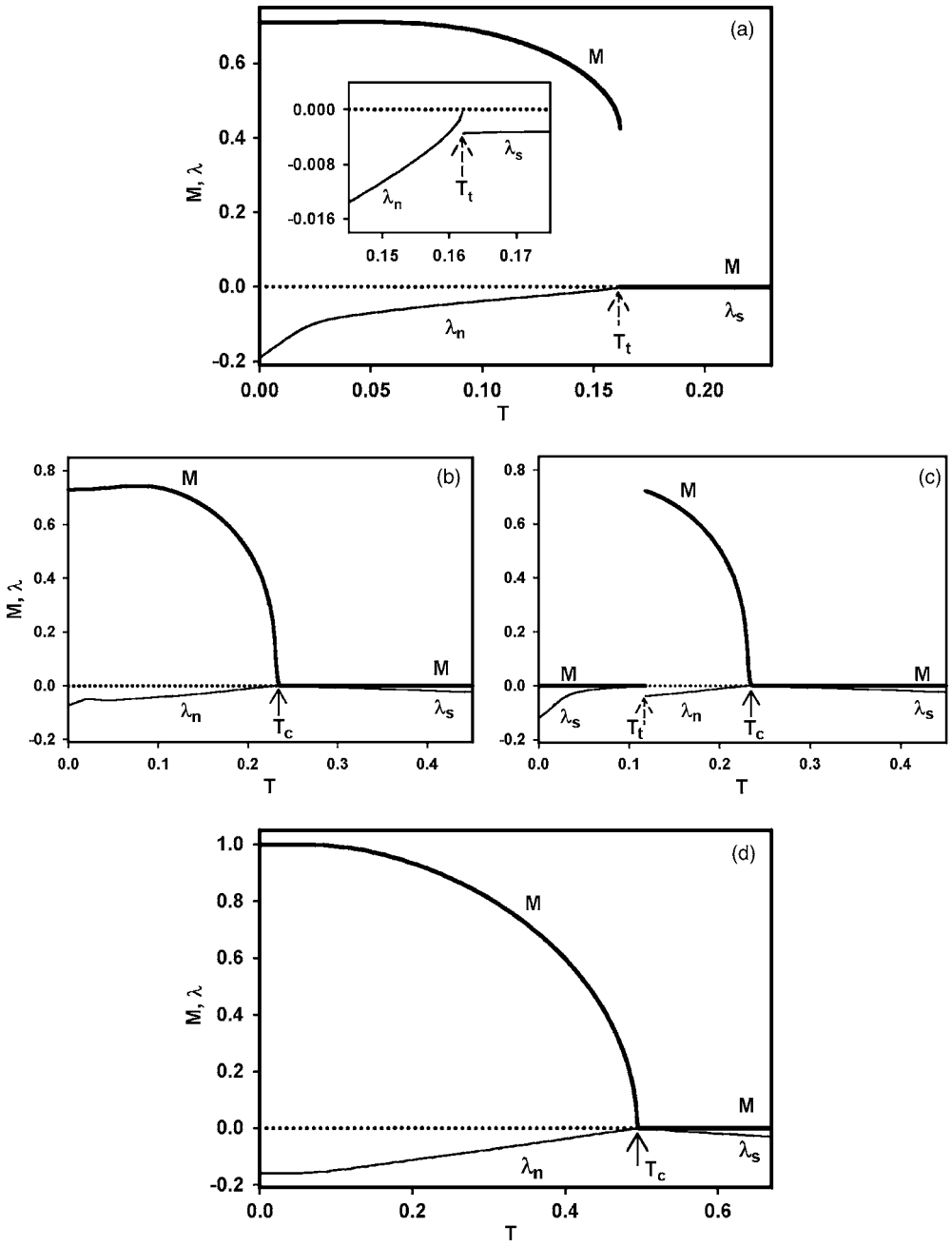

FIG. 3. The reduced temperature dependence of the average magnetization M (the thick solid line) and the Liapunov exponents λ_s and λ_n (the thin solid line), the subscript s indicates a symmetric solution that corresponds to the P phase and n a nonsymmetric solution that corresponds to the F phase. T_t and T_c are the first- and second-order phase transition temperatures, respectively. The F+P region exists for $d=-0.25$ and $h=0.725$. (a) A first-order phase transition for $d=-0.25$ and $h=0.75$; 0.1620 is found T_t. (b) A second-order phase transition for $d=-0.25$ and $h=0.725$; 0.2350 is found T_c. (c) Two successive phase transitions: the first one a first-order and the second one a second-order phase transition for $d=-0.25$ and $h=0.725$; 0.1175 and 0.2350 are found T_t and T_c, respectively. (d) A second-order phase transition for $d=-0.25$ and $h=0.4$; 0.4950 is found T_t.

$=0.495$, and the results are presented in Figs. 4(a)–4(d) respectively; the thick solid line corresponds to M and the thin line is the Liapunov exponent λ. In these figures, values of d are the same as in Fig. 3 and the values of T are chosen DPT points that are obtained in Fig. 3 (compare Fig. 3 with Fig. 4). If one compares Fig. 4 with Fig. 3, one can see that the behavior of M as a function of h (Fig. 4) is exactly the same as the behavior of M as a function of T (Fig. 3). We should also mention that $T_c=0.2350$ in Figs. 3(b) and 3(c) corresponds to Fig. 4(b) and $T_t=0.1175$ in Fig. 3(c) corresponds to Fig. 4(c). Since we have explained Fig. 3 in detail, we will not elucidate Fig. 4. At this point, we should also mention that since we calculated and plotted only one type of solution, either paramagnetic or ferromagnetic, in Figs. 3 and 4, the discontinuity occurs for λ_s at T_t. On the other hand, if one computes and presents both solutions together, one finds that

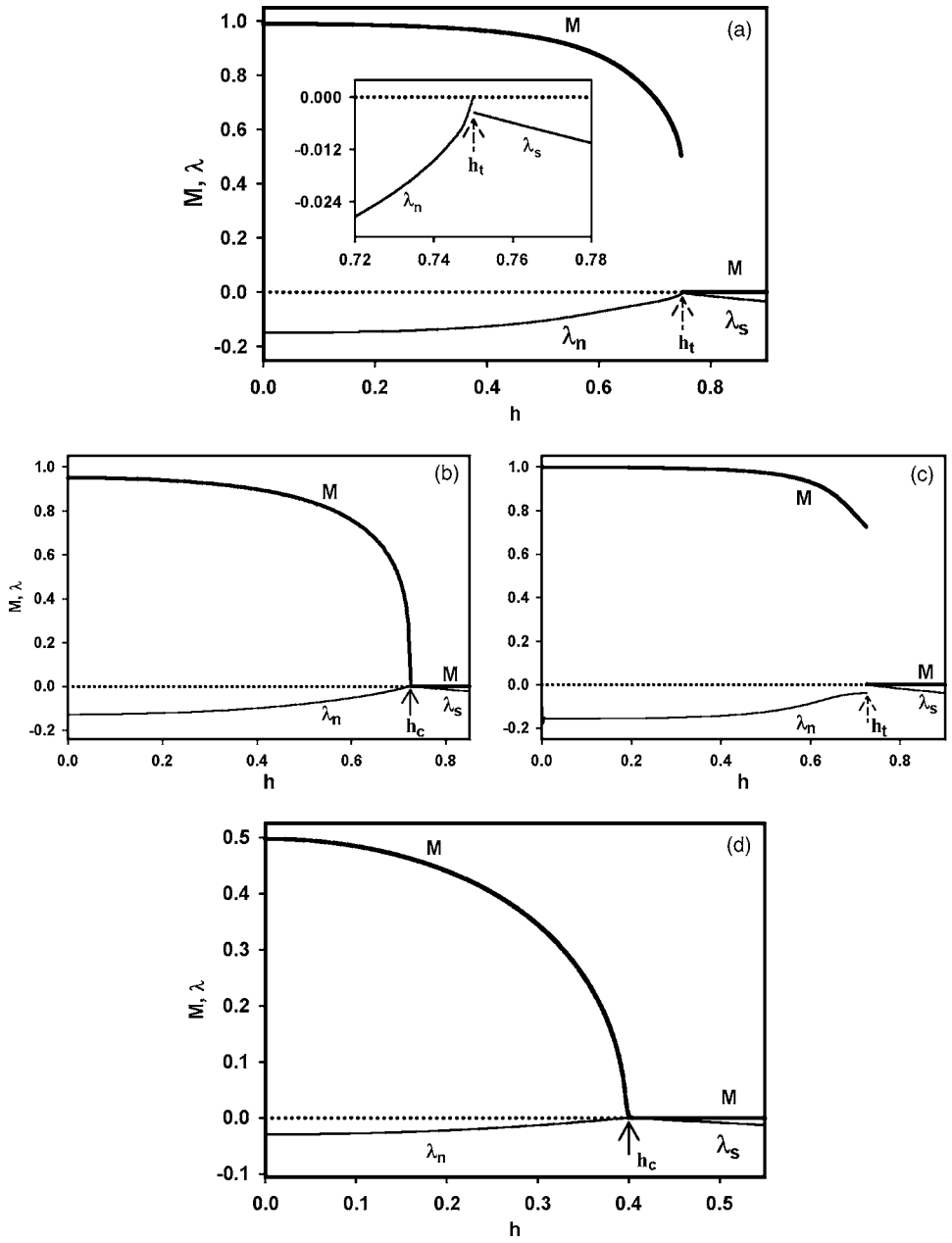

FIG. 4. Same as Fig. 3, but the reduced external magnetic field dependence of the average magnetization M and the Liapunov exponents λ_s and λ_n. (a) $d=-0.25$ and $T=0.1620$. The first-order phase transition occurs for $h=0.75$. (b) $d=-0.25$ and $T=0.2350$. The second-order phase transition occurs for $h=0.725$. (c) $d=-0.25$ and $T=0.1175$. The first-order phase transition occurs for $h=0.725$. (d) $d=-0.25$ and $T=0.4950$. The second-order phase transition occurs for $h=0.40$.

λ_s is always continuous. This fact is illustrated in Fig. 5. The similar behavior of Fig. 5(b) was also found by Tomé and Oliveira [18] (compare Fig. 5(b) with Fig. 4 in Ref. [18]).

Finally, it is worthwhile to mention that in order to see the influence of the oscillating external magnetic field, we have done the calculations for static h. Figure 6(a) shows the thermal variations of M and λ for several values of static h and $d=-0.25$. Figure 6(b) represents the behaviors of M and λ as a function of static h for $d=-0.25$ and several values of T. One can see from these figures that the system does not undergo any phase transitions for static h. Hence, we have concluded that the oscillating external magnetic field induced the phase transitions.

We can now obtain the phase diagrams of the system and the calculated phase diagrams in the (T,h) plane are presented in Figs. 7(a)–7(e). In these phase diagrams the solid and dashed lines represent the second- and first-order phase transition lines, respectively, the dynamic tricritical points are denoted by filled triangles. For the positive values of d, only one type of phase diagram is obtained, seen in Fig. 7(a), and when we extended the d values to negative values, four different phase diagrams are found, illustrated in Figs. 7(b)–7(e).

Figure 7(a) represents the phase diagram for the positive values of d, i.e., $d=0.25$. In this phase diagram, at high reduced temperature (T) and reduced external magnetic field (h) the solutions are paramagnetic, and at low values of T and h they are ferromagnetic. The boundary between these regions, $F \rightarrow P$, is the second-order phase line. At low reduced temperatures, there is a range of values of h in which the P and the F phases or regions coexist, called the coexistence region, F+P. The F+P region is separated from the F and the P phases by the first-order phase line. The system also exhibits only one dynamic tricritical point where both

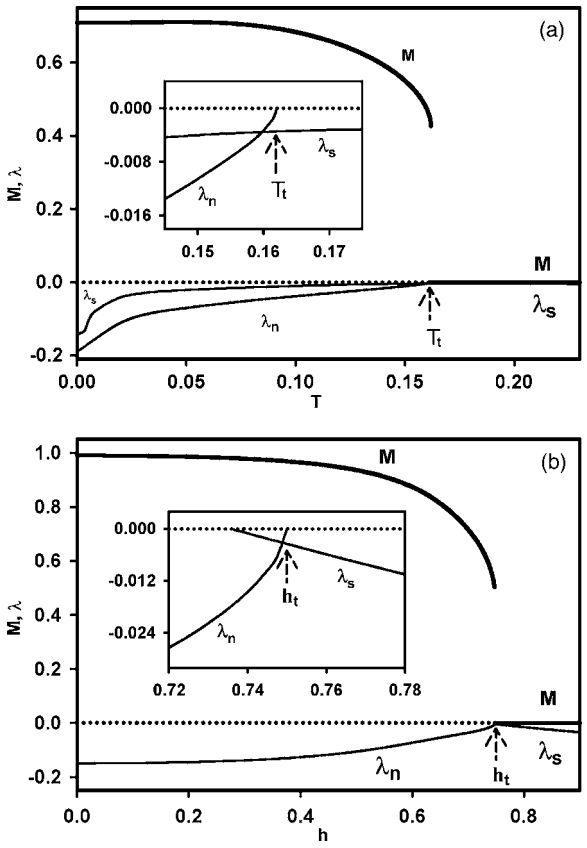

FIG. 5. (a) Same as Fig. 3(a), but we present the both solutions together and λ_s becomes continuous. (b) Same as Fig. 4(a), but we present the both solutions together and λ_s becomes continuous.

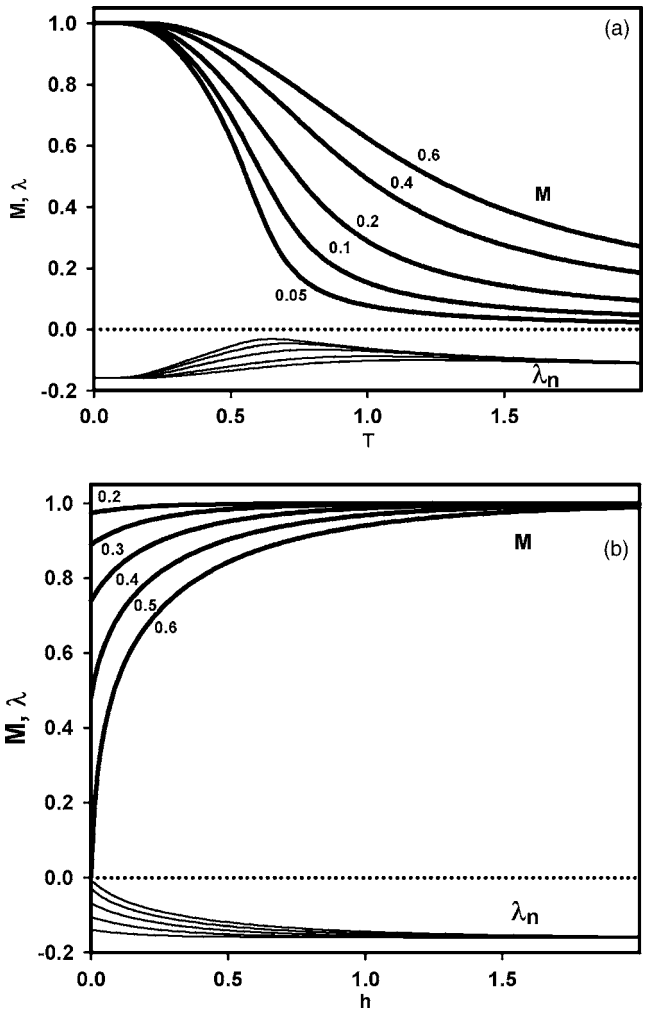

FIG. 6. (a) Thermal variations of M and λ_n for several values of static h and $d=-0.25$. The number accompanying each curve denotes the value of static h. (b) The behaviors of M and λ_n as function of static h for $d=-0.25$. The number accompanying each curve denotes the value of T.

first-order phase transition lines merge and signals the change from a first- to a second-order phase transitions. Finally, we should also mention that similar phase diagrams were also obtained in the kinetic of the mixed spin-1/2 and spin-1 Ising ferromagnetic system [19] as well as the kinetic spin-1/2 Ising model [18]. The reason that the phase diagram is similar to the one obtained for the kinetic spin-1/2 Ising model is due to the competition between J, d, and h. If $d>0$, the Hamiltonian of the spin-1 model gives similar results to the Hamiltonian of the spin-1/2 Ising model. This can be seen explicitly from the ground-state phase diagrams that were obtained in detail by Morita [27]. More explicitly, for $d>0$, $S_i=\pm 1$ states appear, but the $S_i=0$ state does not appear in the ground-state phase diagram (see Fig. 2(a) of Ref. [27]).

We now turn to the interesting situation when d values are negative. In this case, four different phase diagram topologies are found, which depend on d values.

(i) For $-0.0104>d\geqslant-0.4654$, the phase diagram is similar to Fig. 7(a) but only differs from Fig. 7(a) in that for very low T and h values, one more P+F coexistence region also exists. The boundary between this F+P region and the F phase is the first-order line, seen in Fig. 7(b). A similar phase diagram was also obtained in kinetics of the mixed Ising ferrimagnetic system [19].

(ii) For $-0.4654>d\geqslant-0.5543$, the system exhibits two dynamic tricritical points. One of them occurs in similar places in Figs. 7(a) and 7(b), and the other occurs in the low values of h, seen in Fig. 7(c). The latter dynamic tricritical point occurs as follows. The second-order phase line between the F and P phases does not end at $h=0$. It merges the first-order phase boundary between the regions of F and P +F, hence, the second dynamic tricritical point occurs. Moreover, the first-order phase transition lines exist at the low reduced temperatures, and h values separate not only the P+F region from the F phase, but also from the P phase, seen explicitly in Fig. 7(c).

(iii) For $-0.5543>d\geqslant-0.9891$, the phase diagram is obtained for $d=-0.625$, seen in Fig. 7(d). This is the more interesting phase diagram in which besides, the two dynamic tricritical points existing in the system, at low reduced temperatures there is a range of h wherein the paramagnetic phase also occurs. The system has three different the F+P regions at low reduced temperatures in addition to the P and F phases, seen in Fig. 7(d).

(iv) For $-0.9891>d$, the phase diagram is presented for $d=-1.0$, seen in Fig. 7(e), and is similar to case (iii), except

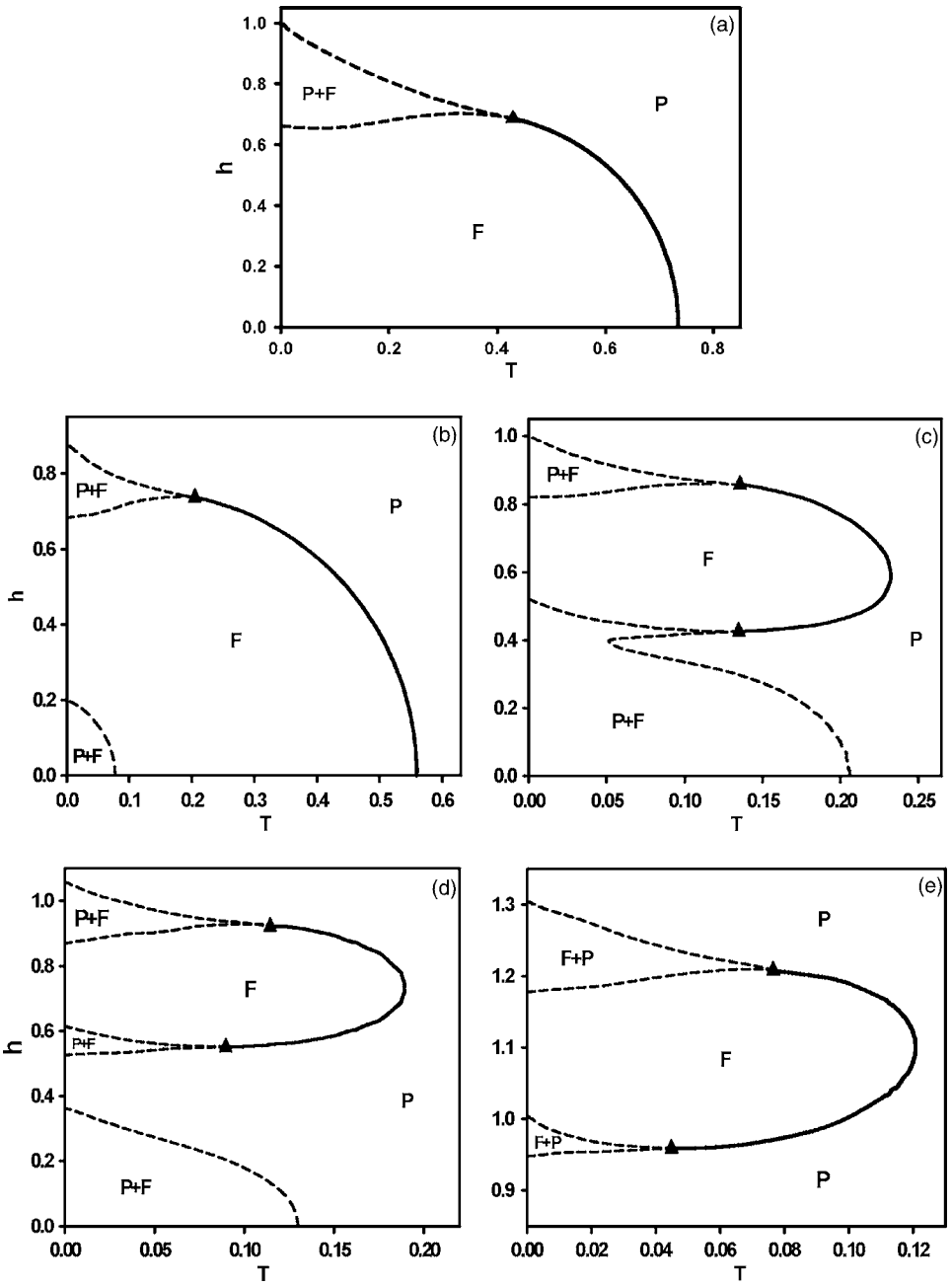

FIG. 7. Phase diagrams of the Blume-Capel model in the (T,h) plane. Paramagnetic, Ferromagnetic, and the coexistence region (F+P) are found. Dashed and solid lines represent the first- and second-order phase transitions, respectively, and the dynamic tricritical points are indicated with filled triangles. (a) $d=0.25$, (b) $d=-0.25$, (c) $d=-0.525$, (d) $d=-0.625$, and (e) $d=-1.0$.

that the P+F region at low values of T and h disappears [compare Fig. 7(e) with Fig. 7(d)]. It is worthwhile to mention that the similar phase diagram was also found in the kinetics of the mixed Ising ferrimagnetic system [19]. Finally, it is worthwhile to mention that for $d<0$, the phase diagrams are not similar to the one obtained for the kinetic spin-1/2 Ising model. This fact can also be seen from the ground-state phase diagram of the spin-1 Ising model in which, for $d<0$, all the states, namely, $S_i=\pm 1,0$, play the role in the system (see Fig. 2(a) of Ref. [27]).

V. SUMMARY AND CONCLUSIONS

We have analyzed within a mean-field approach the stationary states of the kinetic spin-1 Blume-Capel model under a time-dependent oscillating external magnetic field. We use a Glauber-type stochastic dynamic to describe the time evolution of the system. We have studied the behavior of the time dependence of the magnetization and the behavior of the average magnetization as a function of reduced temperature and the reduced external magnetic field. The DPT points are found and the phase diagrams presented in the (T,h) plane. We have also calculated the Liapunov exponent to verify the stability of a solution and the DPT points.

We found that the behavior of the system strongly depends on the values of the crystal field interaction or a single-ion anisotropy D (we used the reduced crystal field interaction $d=D/Jz$). For positive values of d, the system behaves as kinetics of a mixed spin-1/2 and spin-1 Ising ferromagnetic system [19] and also the kinetic spin-1/2 Ising model [18]; it has a second-order phase transition at high T

and low h. As T decreases and h increases, the transition becomes a first-order one the system presents a dynamic tricritical point, and the F+P coexistence region exists, seen in Fig. 7(a). For small negative values of d, the phase diagram is similar to Fig. 7(a); the difference at low values of T and h in which the F+P region occurs in the system, is seen Fig. 7(b). In this case, the system behaves as the kinetics of a mixed Ising ferromagnetic system [19]. However, when d is large and negative, an interesting phase diagram has been obtained. In this case, the system exhibits two dynamic tricritical points and first-order phase transitions lines appear at low reduced temperatures, seen in Fig. 7(c). When d is large enough and negative, very interesting phase diagram has been obtained [see Fig. 7(d)]. Figure 7(d) is similar to Fig. 7(c), except at low reduced temperatures, the P phase exists in addition to the F phase and three different F+P regions. For $d<-0.9891$, the phase diagram is similar to Fig. 7(d), except the P+F region at low values of T and h disappears [compare Fig. 7(d) with Fig. 7(e)].

The reason another P+F phase at low T and h appears in the phase diagrams is as follows: For low values of T and h, due to the competition between T, h, and the decreasing d time-dependent magnetization either follows the reduced external magnetic field within a single period, and $M=0$ (this is the disordered or paramagnetic solution), or it cannot fully switch sign within a single period, and $|M|>0$ (this is the ordered or ferromagnetic solution). These behaviors are similar to Fig. 2. On the other hand, for large and negative d, the paramagnetic phase becomes larger. This fact can also be seen analytically. When decreasing d, the second term in the right-hand side of Eq. (11) disappears. Hence, the solution of time-dependent magnetization is $m(\xi)\sim e^{-\xi/\Omega}$. When $\xi\rightarrow\infty$, the stationary solution of $m(\xi)$ always corresponds to the paramagnetic solution or phase. Moreover, if one chooses suitable values for h and initializing M appropriately, at low reduced temperatures, the crystal field interaction dominates until T_t, and then the bilinear interaction dominates. This fact can be seen in Fig. 3(c) and Figs. 7(b)–7(e).

Finally, we should also mention that this mean-field dynamic study suggests that spin-1 Blume-Capel model in the presence of a time-dependent oscillating external magnetic field has an interesting dynamic behavior, quite different from the standard Ising model. Therefore, it would be worthwhile to further study it with more accurate techniques such as dynamic Monte Carlo simulations or renormalization group (RG) calculations. Particularly, the real space [28] RG technique [29] was proposed by Achiam [30] and Achiam and Kosterlitz [31]. This method was also used to study the dynamics of the one-dimensional Blume-Emery-Griffiths model; in particular, critical relaxation of the model was analyzed [32].

ACKNOWLEDGMENTS

The final stage of this work was supported by the Technical Research Council of Turkey (TÜBİTAK) Grant No. 105T114.

[1] M. Blume, Phys. Rev. **141**, 517 (1966).
[2] H. W. Capel, Physica (Utrecht) **32**, 966 (1966); **33**, 295 (1967).
[3] D. Mukamel and M. Blume, Phys. Rev. A **10**, 610 (1974); M. Blume, V. J. Emery, and R. B. Griffiths, *ibid.* **4**, 1071 (1971).
[4] D. M. Saul, M. Wortis, and D. Stauffer, Phys. Rev. B **9**, 4964 (1974); J. Oitmaa, Phys. Lett. **33A**, 230 (1970); J. Oitmaa, J. Phys. C **5**, 435 (1972); J. G. Brankov, J. Przystawa, and E. Praveczki, *ibid.* **5**, 3387 (1972).
[5] D. H. Y. Yang and Y. L. Wang, Phys. Rev. B **12**, 1057 (1975).
[6] B. L. Arora and D. P. Landau, AIP Conf. Proc. **10**, 870 (1973); A. K. Jain and D. P. Landau, Phys. Rev. B **22**, 445 (1980); J. D. Kimel, S. Black, P. Carter, and Y. L. Wang, *ibid.* **35**, 3347 (1986); J. D. Kimel, P. A. Rikvold, and Y. L. Wang, *ibid.* **45**, 7237 (1992).
[7] Th. W. Burkhardt, Phys. Rev. B **14**, 1196 (1976); E. K. Riedel and F. J. Wegner, Phys. Rev. Lett. **29**, 349 (1972); E. K. Riedel and F. J. Wegner, Phys. Rev. B **7**, 248 (1973); E. K. Riedel and F. J. Wegner, Phys. Rev. B **9**, 294 (1974); G. D. Mahan and S. M. Girvin, Phys. Rev. B **17**, 4411 (1978); A. Brognara, A. Parola, and L. Reatto, Phys. Rev. E **65**, 066113 (2002).
[8] T. Kaneyoshi, J. Phys. C **19**, L557 (1986); T. Kaneyoshi, J. Phys. C **21**, L679 (1988); Y. L. Wang and C. Wenthworth, J. Appl. Phys. **61**, 4411 (1987); M. Jurčišin, A. Bobák, and M. Jaščur, Physica A **224**, 684 (1996);
[9] C. Buzano and A. Pelizzola, Physica A **216**, 158 (1995); T. Balcerzak and J. W. Tucker, J. Magn. Magn. Mater. **278**, 87 (2004).
[10] S. Grollau, E. Kierlik, M. L. Rosinberg, and G. Tarjus, Phys. Rev. E **63**, 041111 (2001).
[11] A. Du, Y. Q. Yü, and H. J. Liu, Physica A **320**, 387 (2003).
[12] C. Ekiz, Phys. Lett. A **324**, 114 (2004).
[13] T. Fiig, B. M. Gorman, P. A. Rikvold, and M. A. Novotny, Phys. Rev. E **50**, 1930 (1994).
[14] F. Manzo and E. Olivieri, J. Stat. Phys. **104**, 1029 (2001).
[15] C. Ekiz, M. Keskin, and O. Yalçin, Physica A **293**, 215 (2001).
[16] R. Kikuchi, Suppl. Prog. Theor. Phys. **35**, 1 (1966).
[17] R. J. Glauber, J. Math. Phys. **4**, 294 (1963).
[18] T. Tomé and M. J. de Oliveira, Phys. Rev. A **41**, 4251 (1990).
[19] G. M. Buendía and E. Machado, Phys. Rev. E **58**, 1260 (1998).
[20] J. F. F. Mendes and E. J. S. Lage, J. Stat. Phys. **64**, 653 (1991).
[21] M. Acharyya, Phys. Rev. E **56**, 2407 (1997); A. Chatterjee and B. K. Chakrabarti, *ibid.* **67**, 046113 (2003).
[22] S. W. Sides, P. A. Rikvold, and M. A. Novotny, Phys. Rev. Lett. **81**, 834 (1998); Phys. Rev. E **59**, 2710 (1999); G. Korniss, C. J. White, P. A. Rikvold, and M. A. Novotny, *ibid.* **63**, 016120 (2000); G. Korniss, P. A. Rikvold, and M. A. Novotny, *ibid.* **66**, 056127 (2002).
[23] B. K. Chakrabarti and M. Acharyya, Rev. Mod. Phys. **71**, 847 (1999).
[24] M. Zimmer, Phys. Rev. E **47**, 3950 (1993); M. Acharyya and

B. K. Chakrabarti, Phys. Rev. B **52**, 6550 (1995); M. Acharyya, Phys. Rev. E **58**, 179 (1998); H. Fujisaka, H. Tutu, and P. A. Rikvold, *ibid.* **63**, 036109 (2001).
[25] H. Tutu and N. Fujiwara, J. Phys. Soc. Jpn. **73**, 2680 (2004).
[26] Q. Jiang, H. N. Yang, and G. C. Wang, Phys. Rev. B **52**, 14911 (1995); Q. Jiang, H. N. Yang, and G. C. Wang, J. Appl. Phys. **79**, 5122 (1996).
[27] T. Morita, Phys. Lett. A **133**, 369 (1988).
[28] T. Niemeijer and M. J. van Leeuwen, in *Phase Transitions and Critical Phenomena*, edited by C. Domb and M. S. Green (Academic, New York, 1976), Vol. 6.
[29] K. G. Wilson and J. Kogut, Phys. Lett., C **12**, 75 (1974).
[30] Y. Achiam, Physica A **120**, 279 (1983).
[31] Y. Achiam and J. M. Kosterlitz, Phys. Rev. Lett. **41**, 128 (1978).
[32] Y. Achiam, Phys. Rev. B **31**, 260 (1985).